

Article

## ***In Situ* Monitoring of Temperature inside Lithium-Ion Batteries by Flexible Micro Temperature Sensors**

**Chi-Yuan Lee \*, Shuo-Jen Lee, Ming-Shao Tang and Pei-Chi Chen**

Department of Mechanical Engineering, Yuan Ze Fuel Cell Center, Yuan Ze University, 135 Yuan-Tung Road, Chung-Li, Taoyuan 32003, Taiwan; E-Mails: mesjl@saturn.yzu.edu.tw (S.-J.L.); gefb3954@gmail.com (M.-S.T.); peggy416420@gmail.com (P.-C.C.)

\* Author to whom correspondence should be addressed; E-Mail: cylee@saturn.yzu.edu.tw; Tel.: +886-3-4638-800 ext 2478; Fax: +886-3-455-8013.

Received: 29 August 2011; in revised form: 18 October 2011 / Accepted: 18 October 2011 / Published: 21 October 2011

---

**Abstract:** Lithium-ion secondary batteries are commonly used in electric vehicles, smart phones, personal digital assistants (PDA), notebooks and electric cars. These lithium-ion secondary batteries must charge and discharge rapidly, causing the interior temperature to rise quickly, raising a safety issue. Over-charging results in an unstable voltage and current, causing potential safety problems, such as thermal runaways and explosions. Thus, a micro flexible temperature sensor for the in *in-situ* monitoring of temperature inside a lithium-ion secondary battery must be developed. In this work, flexible micro temperature sensors were integrated into a lithium-ion secondary battery using the micro-electro-mechanical systems (MEMS) process for monitoring temperature *in situ*.

**Keywords:** MEMS; micro temperature sensor; lithium-ion secondary battery; *in situ* monitoring

---

### **1. Introduction**

In recent years, lithium-ion secondary batteries have been extensively used in commercial products, such as smart phones, personal digital assistants (PDA), notebooks and electric cars. Given this widespread use, the safety and efficiency of lithium-ion secondary batteries are important issues.

The safety of a lithium-ion secondary battery depends on the electrolyte, separator, anode and cathode [1]. Under overcharge conditions, lithium forms an active surface and reacts with the

electrolyte, increasing internal impedance and reducing discharge efficiency. With increasing charge-discharge cycles, the capacity of the battery will decrease, limiting its cycle life.

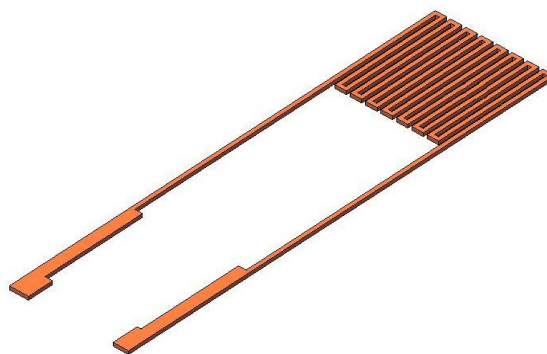
Metallic lithium can separate out in the form of dendrite and acicular crystals and cause many problems during rapid charging and discharging [2]. Accordingly, the efficiency of the battery is reduced, and a problem of safety arises [3,4]. The internal temperature of a lithium-ion secondary battery is typically measured using a thermocouple. Traditional thermocouples are too large to be able to be used to accurately determine the temperature at an optimal measurement position [5]. Damage to the battery during temperature measurement should be avoided. A four-probe electrical technique that is both fast (<200 ms) and accurate ( $\pm 0.1$  °C) and works by connecting to the two terminals of the cell [6], eliminates the need for inserting any probe into the cell. Remote query sensors are used to measure the temperature, pressure, fluid-flow velocity and humidity [7-9]. In this investigation, resistance temperature detector (RTD) micro temperature sensors with small volume, high accuracy, short response time, simplicity of fabrication, mass-producibility, and the capacity to measure the temperature more effectively than traditional thermocouples, are utilized. These micro temperature sensors must be resistant to erosion, high temperature and stress corrosion.

## 2. Methodology

### 2.1. Design of a Micro Temperature Sensor

Temperature sensors fall into four main classes—gold RTDs, thermally sensitive resistors (thermistors), thermocouples, and mercury-in-glass thermometers. The micro temperature sensor that is fabricated herein is a gold RTD, and is illustrated in Figure 1.

**Figure 1.** Schematic diagram of a micro temperature sensor.



The resistance of a general metal is given by:

$$R = \rho L / A \quad (1)$$

where  $R$  denotes resistance ( $\Omega$ );  $\rho$  presents resistivity ( $\Omega\text{m}$ );  $L$  denotes wire length (m), and  $A$  denotes cross-sectional area ( $\text{m}^2$ ). When the temperature of the RTD varies in the linear region, the relationship between the measured resistance and the change in temperature can be expressed as:

$$R_t = R_i (1 + \alpha_i \Delta T) \quad (2)$$

$$\Delta T = t - t_i \quad (3)$$

where  $R_t$  and  $R_i$  represent the resistance of an RTD at  $t$  °C and  $t_i$  °C, respectively;  $\alpha_t$  represents the positive temperature coefficient of an RTD;  $\Delta T$  denotes the variation in temperature from the reference temperature; and  $t$  and  $t_i$  are the temperature of an RTD at  $t$  °C and  $t_i$  °C, respectively. Equation (2) can thus be rewritten as

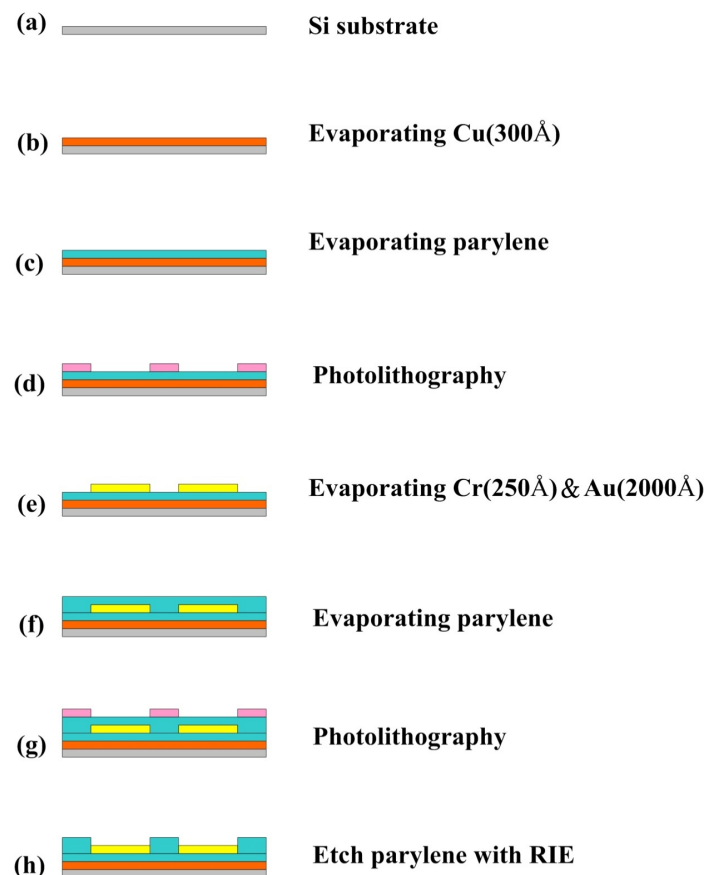
$$\alpha_t = \frac{R_t - R_i}{R_i(\Delta T)} \quad (4)$$

where  $\alpha_t$  is the temperature coefficient of resistance (TCR) of the sensor.

## 2.2. Fabrication of Micro Temperature Sensor

In this study, parylene, in the form of a thin film, was adopted as a flexible micro temperature sensor. Parylene is resistant to erosion and stress corrosion. The sensor material was deposited layer-by-layer by the physical vapor deposition (PVD) technique; thus, the micro temperature sensors could be fabricated at low temperature with accurately controlled thickness. Figure 2 presents the eight steps (a–h) involved in fabricating the sensor.

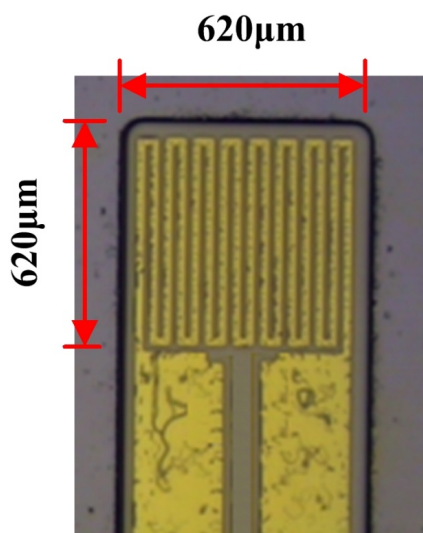
**Figure 2.** Procedure for fabricating flexible micro temperature sensors on silicon substrate.



Steps a and b: a layer of copper (Cu) was deposited as a sacrificial layer on a silicon wafer substrate, and then a 300 Å-thick parylene thin film was deposited onto the layer of copper, as displayed. Step c: the parylene thin film acted as a protective layer, an isolation layer and a substrate. Step d: the first lithographic process was carried out with the purpose of defining the pattern on the micro temperature sensors. Step e: Cr (250 Å) and then Au (2000 Å) were deposited on the parylene substrate as a

conduction layer using an e-beam evaporator. The structure of the micro temperature sensors was formed with the lift-off process. Step f: then, another parylene layer was deposited to protect the micro temperature sensors. Steps g and h: the second lithographic process, reactive ion etching (RIE), defined the pattern on the contact pads and in the sensing region. Figure 3 shows an optical microscope (OM) image of the micro temperature sensor.

**Figure 3.** Optical microscopic photograph of the flexible micro temperature sensor.



### 3. Results and Discussion

#### 3.1. Calibration of Micro Temperature Sensors

The micro temperature sensor was placed in a thermal chamber (DENG YNG DS-45), as presented in Figure 4.

**Figure 4.** Calibration of micro temperature sensors in a thermal chamber.



The resistance signal was picked up by a Data Acquisition system, as displayed in Figure 5. The temperature of the thermal chamber was increased from  $-20\text{ }^{\circ}\text{C}$  to  $90\text{ }^{\circ}\text{C}$  three times.

Figure 5. Resistance signal is picked up by Data Acquisition.



Figures 6 and 7 plot the calibration curves of the micro temperature sensor. The calibration curve exhibits high repeatability and linearity of the relationship between temperature and resistance.

Figure 6. Calibration curves of sensor 1.

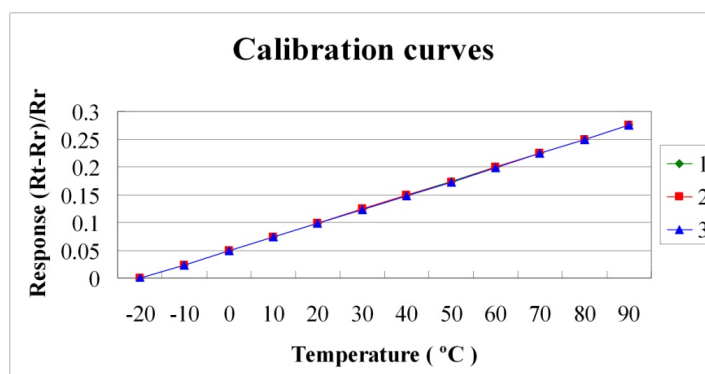
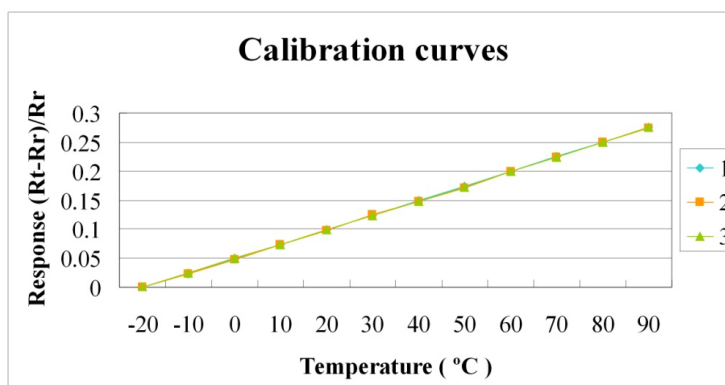


Figure 7. Calibration curves of sensor 2.



### 3.2. Thermal Shock Test

An experiment was conducted to test the strength of the micro temperature sensor structure using a Programmable Thermal Shock Tester wherein a sensor placed inside the tester measured and reported the temperature. The temperatures were cycled three times between 0 °C and 90 °C by ramping the temperatures over a period of 3 minutes with a 5 minutes dwell-time at each extreme temperature. In Figure 8, T1 is the temperature curve of space in the Programmable Thermal Shock Tester, T2 is the temperature curve of holder placed micro temperature sensor 1. Figure 9 plots the calibration curve of micro temperature sensor 1.

**Figure 8.** Temperature change of space in Programmable Thermal Shock Tester and holder of micro temperature sensor 1.

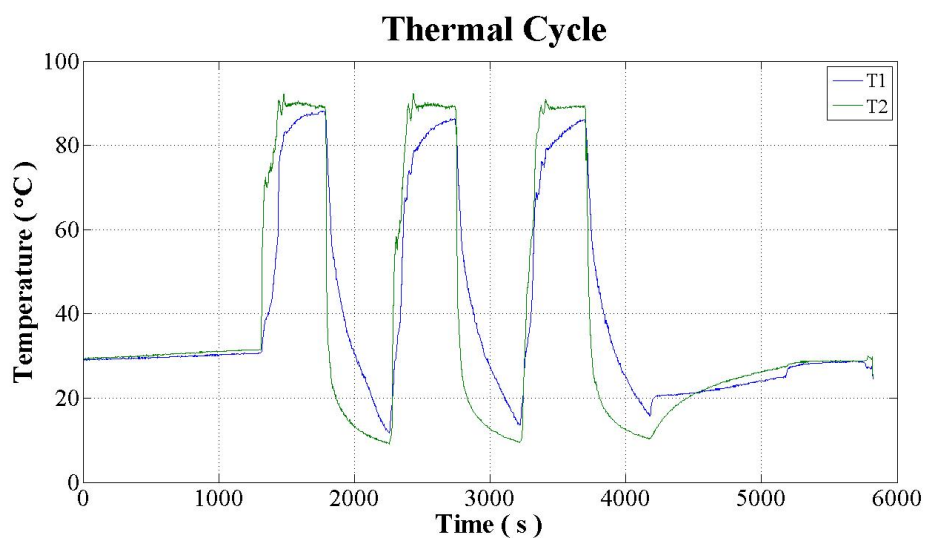
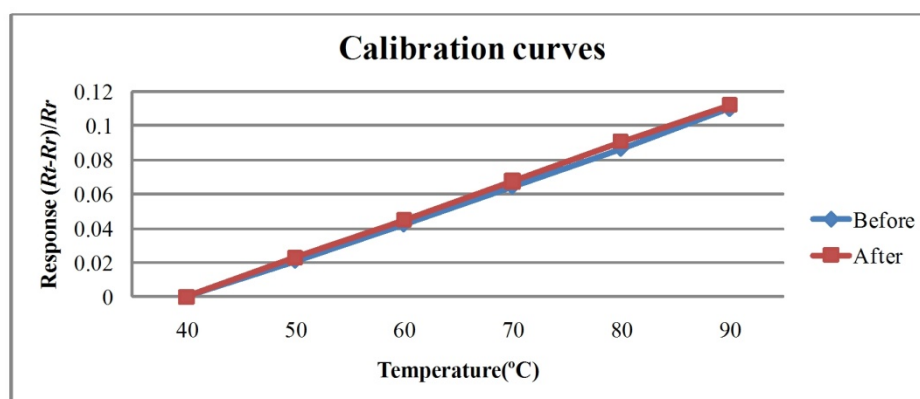


**Figure 9.** Comparison of micro temperature sensor 1 calibration curves before and after thermal shock testing for three cycles.



### 3.2. Temperature Measurement in IC Charging and Discharging

The micro temperature sensors are inserted into a lithium-ion secondary battery, as shown in Figures 10 and 11. A thermocouple attached to the outer surface of the battery measured the surface temperature. The signals from the micro sensors and the thermocouple were picked up by the Data Acquisition system GBT-2211.

**Figure 10.** Micro temperature sensor is inserted into lithium-ion secondary battery.

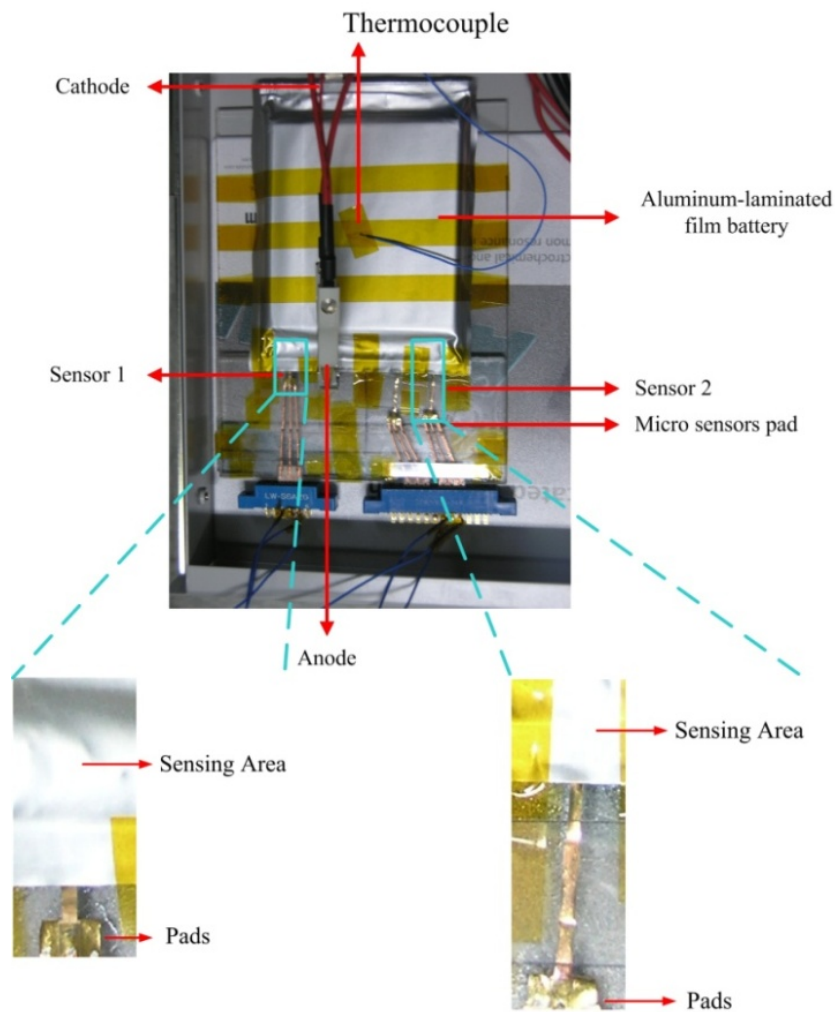


**Figure 11.** Position of micro temperature sensors in lithium-ion secondary battery.

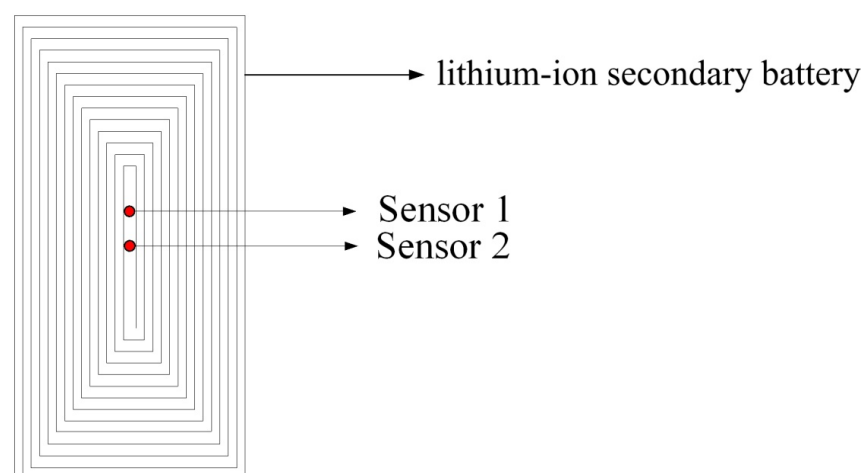
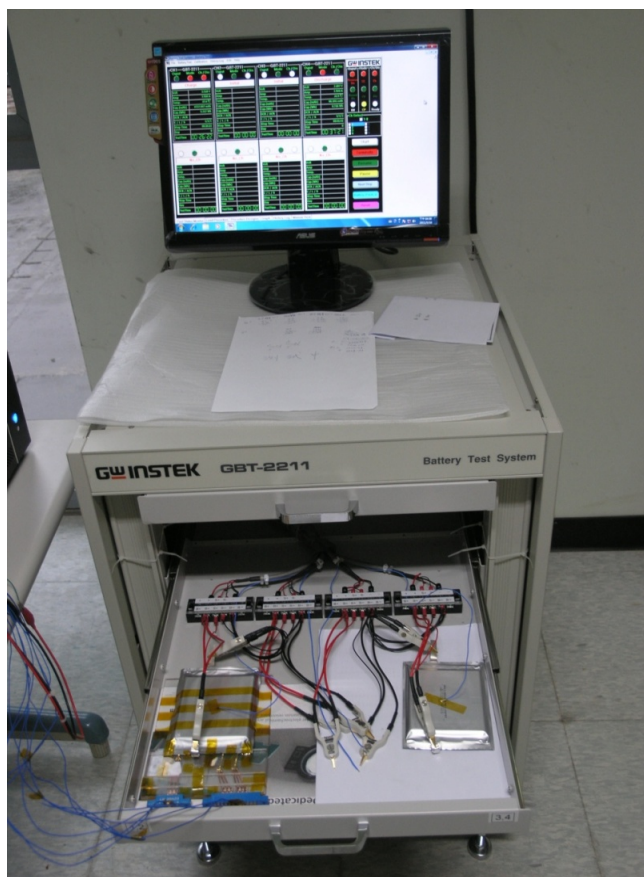


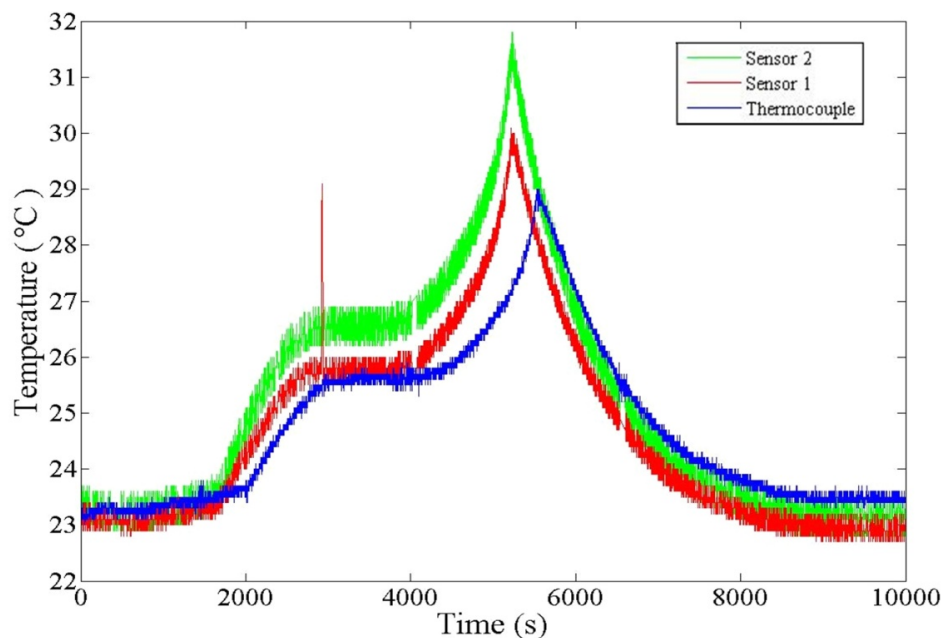
Figure 12 shows the battery tester used in charging and discharging the lithium-ion battery. Figure 13 plots the temperature curve of the thermocouple and the micro temperature sensors. The three curves are all mutually consistent. The temperatures vary among different positions in the lithium-ion secondary battery. The inner temperature changes more rapidly than the outer temperature. At the peak, the inner temperature is 2 °C higher than the outer one.



**Figure 12.** GBT-2211 is used to charge and discharge and lithium-ion secondary battery.



**Figure 13.** Temperature curve during 1C charging and discharging.



#### 4. Conclusions

In this study, parylene is selected as a flexible material to fabricate micro temperature sensors. The strength of the micro temperature sensor suffices for a lithium-ion secondary battery. The *in situ* measurements of temperature are picked up successfully. The results demonstrate that when the



lithium battery 1C charging and discharging reactions occur in the battery, the inner temperature is 2 °C higher than the outer one.

### Acknowledgements

This work was accomplished with much needed support and the authors would like to thank the National Science Council of Taiwan through the grant NSC 99-2632-E-155-001-MY3. The authors also like to thank EXA Energy Technology Company and Ming-Yu Chung and Kuo-Chang Han of the Yuan Ze University for their valuable advice and assistance in experiment. In addition, we would like to thank the YZU NENS Common Lab, TKU MEMS Lab for providing access to their research facilities.

### References

1. Scrosati, B.; Garche, J. Lithium batteries: Status, prospects and future. *J. Power Sour.* **2010**, *195*, 2419-2430.
2. Chen, Z.; Qin, Y.; Amine, K. Redox shuttles for safer lithium-ion batteries. *Electro. Acta* **2009**, *54*, 5605-5613.
3. Delmas, C.; Trier, M.M.; Croguennec, L.; Levasseur, S.; Pérès, J.P.; Poullierie, C.; Prado, G.; Fournès, L.; Weill, F. Lithium batteries: A new tool in solid state chemistry. *Int. J. Inorg. Mater.* **1999**, *1*, 11-19.
4. Fericola, A.; Croce, F.; Scrosati, B.; Watanabe, T.; Ohno, H. LiTFSI-BEPyTFSI as an improved ionic liquid electrolyte for rechargeable lithium batteries. *J. Power Sour.* **2007**, *174*, 342-348.
5. Forgez, C.; Do, D.V.; Friedrich, G.; Morcrette, M.; Delacourt, C. Thermal modeling of a cylindrical LiFePO<sub>4</sub>/graphite lithium-ion battery. *J. Power Sour.* **2010**, *195*, 2961-2968.
6. Rengaswamy, S.; Bliss, G.C.; Michael, H.B.; Andrew, C.B. Instantaneous measurement of the internal temperature in lithium-ion rechargeable cells. *Electrochim. Acta* **2011**, *56*, 6198-6204.
7. Jain, M.K.; Schmidt, S.; Mungle, C.; Loisel, K.; Grimes, C.A. Measurement of temperature and liquid viscosity using wireless magneto-acoustic/magneto-optical sensors. *IEEE Trans.* **2009**, *37*, 2767-2769.
8. Jain, M.K.; Schmidt, S.; Ong, K.G.; Mungle, C.; Loisel, K.; Grimes, C.A. Magnetoacoustic remote query temperature and humidity sensors. *Smart Mater. Struct.* **2000**, *4*, 502-510.
9. Grimes, C.A.; Kouzoudis, D. Remote query measurement of pressure, fluid-flow velocity, and humidity using magnetoelastic thick-film sensors. *Sens. Actuat. A* **2000**, *84*, 205-212.

© 2011 by the authors; licensee MDPI, Basel, Switzerland. This article is an open access article distributed under the terms and conditions of the Creative Commons Attribution license (<http://creativecommons.org/licenses/by/3.0/>).